International Journal of Modern Manufacturing Technologies
ISSN 2067–3604, Vol. XVII, No. 2 / 2025
https://doi.org/ 10.54684/ijmmt.2025.17.2.41

PLA/NATURAL HYDROXYAPATITE COMPOSITES FOR POTENTIAL BONE FILLER APPLICATIONS

Che Nor Aiza Jaafar[1], Charles Christopher Sorrell[2], Prevenaa Rajendran[1], Ismail Zainol[3], Yue Jiang[2]

[1]Department of Mechanical and Manufacturing Engineering, Faculty of Engineering, Universiti Putra Malaysia, 43000 Serdang Selangor, Malaysia
[2]School of Materials Science and Engineering, Hilmer Building, University New South Wales, Sydney, New South Wales, 2052, Australia
[3]Chemistry Department, Faculty of Science and Mathematics, Universiti Pendidikan Sultan Idris, 35900 Tanjong Malim, Perak, Malaysia.

Corresponding author: Che Nor Aiza Jaafar, cnaiza@upm.edu.my

Abstract. This research explores the use of biogenic hydroxyapatite (HAp) derived from fish scales (FsHAp) as an eco-friendly filler in poly(lactic acid) (PLA) composites intended for biomedical purposes. Although PLA/HAp composites have been extensively studied, the utilization of fish-scale-derived HAp remains relatively underreported. In this study, FsHAp particles (~10 μm) obtained from tilapia scales were incorporated into a PLA matrix at concentrations of 10 to 30 wt% through twin-screw extrusion. The resulting composites were characterized in terms of their mechanical, thermal, morphological, and chemical properties. Mechanical performance was examined using tensile, flexural, and impact (Izod) testing. Thermal transitions and molecular interactions were evaluated using differential scanning calorimetry (DSC) and Fourier transform infrared (FTIR) spectroscopy, respectively, while scanning electron microscopy (SEM) provided insights into the microstructural features. Findings revealed that higher FsHAp loading reduced tensile strength, flexural strength, and elongation at break, but enhanced Young's modulus, flexural modulus, and impact resistance. Both FTIR and DSC confirmed interactions between PLA and FsHAp, while SEM showed a homogeneous distribution of particles. Among the formulations, PLA containing 20 wt% FsHAp displayed the most promising properties for biomedical applications, particularly bone tissue engineering. Importantly, all raw materials employed in this work were sourced from renewable origins.

Key words**:** Poly(lactic acid) (PLA), hydroxyapatite (HAp), fish scale hydroxyapatite (FsHAp), PLA/FsHAp composite

1. INTRODUCTION

The growing concern over the environmental impact of conventional petroleum-based polymers has accelerated efforts to identify sustainable alternatives, particularly for biomedical applications. Biodegradable polymers sourced from renewable feedstocks present a promising solution, as they can reduce fossil fuel dependency and lower greenhouse gas emissions. Among them, poly (lactic acid) (PLA)—produced from natural resources such as corn, starch, and sugarcane [1]—is one of the most extensively investigated. Owing to its biodegradability and biocompatibility, PLA has emerged as a practical substitute for traditional plastics. Its use in medicine has broadened considerably, especially in tissue engineering scaffolds and orthopaedic applications [2]. PLA-based implants, such as fixation plates and screws, have shown successful outcomes in managing jaw fractures without requiring additional reinforcement [3]. Nevertheless, the inherent brittleness of PLA limits its broader clinical utility [4]. Moreover, the polymer's relatively poor surface properties, including restricted cell adhesion and proliferation, further hinder its use in regenerative therapies. To address these challenges, researchers have incorporated reinforcing fillers and bioactive materials into PLA matrices to enhance performance [5].
The use of bioceramic fillers—including alumina, zirconia, bioactive glass, glass ceramics, and hydroxyapatite (HAp)—is well established in biomedical device design due to their excellent mechanical strength and biocompatibility [6]. Hydroxyapatite ($Ca_{10}(PO_4)_6(OH)_2$), the principal calcium phosphate mineral in bone, closely resembles natural hard tissues, making it an attractive choice for bone-interfacing materials and implant coatings

[4]. Mimicking the mechanical behaviour of natural bone is critical for load-bearing applications, and thus HAp is widely employed as a reinforcement phase [7]. Combining HAp ceramics with PLA matrices enables the development of composites that merge toughness with bioactivity, offering significant potential as bone substitutes [8].

Synthetic hydroxyapatite has been extensively applied in biomaterial research owing to its osteoconductivity, bioactivity, and strong biocompatibility [9]. However, chemical synthesis routes are costly, largely due to the use of high-purity precursors [10]. To reduce production costs, natural sources of HAp—such as mammalian bone—have been explored, but their use raises ethical and biosafety concerns. These include the risk of transmitting diseases like bovine spongiform encephalopathy (BSE) and complications with HALAL certification, which is highly relevant to the global Muslim community [11]. As a result, fish scale-derived hydroxyapatite (FsHAp) has emerged as a safer and more acceptable alternative. It is economically viable, free from mammalian origin, and aligns with both health and religious considerations, enhancing its appeal as a biomaterial [12–13].

Despite these advantages, research on incorporating FsHAp into polymeric composites for biomedical use remains limited. Thus, this study focuses on developing PLA/FsHAp composites and examining their mechanical, chemical, thermal, and microstructural characteristics. The findings highlight the potential of these composites, particularly in bone-related applications, as sustainable and biocompatible materials for medical use.

2. MATERIALS AND METHODS

2.1. Materials

PLA (Luminy® LX575) was procured from Total Corbion, Thailand, while fish scale-derived hydroxyapatite (FsHAp) was extracted from Tilapia fish scales, then processed into powder form through ball milling and spray drying. The mixing composition of PLA and FsHAp particles is presented in Table 1.

Table 1. Composition and designation of PLA/FsHAp composites

Sample Code	PLA (wt%)	FsHAp (wt%)
PLA	100	0
PLA/FsHAp10	90	10
PLA/FsHAp20	80	20
PLA/FsHAp30	70	30

A co-rotating twin-screw extruder (Micromag) was employed to compound PLA and FsHAp particles following a pre-mixing process. The composite material was extruded through a four-hole die using the twin-screw machine, operating across ten heating zones set to the following temperatures (from feeder to die): 190, 190, 190, 200, 200, 200, 200, 200, 190, and 180 °C. The extrudate was conveyed along a cooling belt to form continuous composite rods. After extrusion, the PLA/FsHAp composite rods were pelletized at a constant speed of 32 rpm. The resulting pellets were stored in an airtight, dry container at room temperature to prevent moisture absorption prior to hot pressing. Compression molding was then performed using a Technovation hot press machine to produce composite sheets. The PLA/FsHAp pellets were placed into a square mold with a thickness of 3 mm. The mold was pre-heated for approximately 12 minutes at 195 °C, followed by full compression under a pressure of 45 MPa for 10 minutes. The resulting composite sheets were cut into test specimens according to relevant ASTM standards. The detailed steps of the sample preparation process are illustrated in Figure 1.

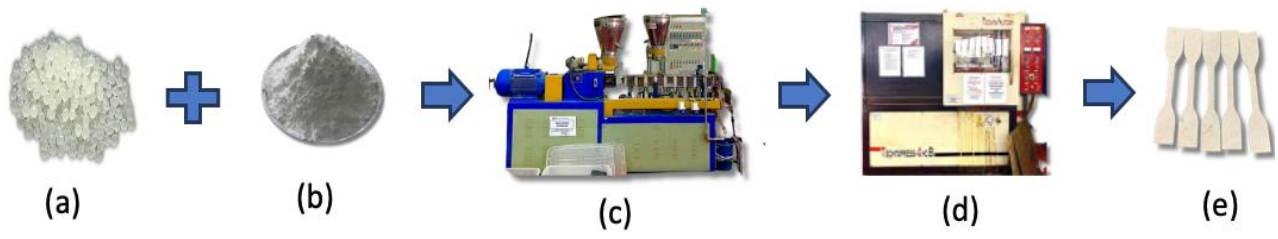

Fig. 1. Process steps in the production of PLA/FsHAp composites: (a) and (b) pre-mixing of PLA and FsHAp powders, (c) compounding and extrusion of PLA/FsHAp particles, (d) compression molding of PLA/FsHAp granules, and (e) preparation of PLA/FsHAp test specimens.

2.2. Tensile Test

Tensile tests were performed according to ASTM D638-14 using an Instron 3365 UTM with a 5 kN load cell at a crosshead speed of 50 mm/min. Sample dimensions were measured with a Mitutoyo caliper, and a 33 mm gauge

length was marked. Five specimens per formulation were tested at room temperature, with average values reported from three valid results.

2.3. Flexural test

Flexural tests were carried out following ASTM D790-17 using an Instron 3366 UTM with a 5 kN load cell and three-point bending fixture. Tests were performed at a crosshead speed of 12 mm/min with a 50 mm support span. Specimen dimensions were measured with a Mitutoyo caliper. Five samples per formulation were tested, and average values were reported.

2.4. Impact Test

Izod impact tests were performed according to ASTM D256-10 using a Ray-Ran impact tester at 3.46 m/s with 2.75 J impact energy. Specimen thickness and V-notch depth were measured with a Mitutoyo caliper. Five samples per formulation were tested, and average impact strength was reported.

2.5. Differential Scanning Calorimetry (DSC)

Thermal behavior of PLA and PLA/FsHAp composites was analyzed using differential scanning calorimetry (Thermo Scientific DSC). About 7 mg of each sample was sealed in a pressure-tight pan and heated from 30 °C to 250 °C at 10 °C/min under nitrogen. Glass transition (Tg), melting (Tm), and crystallization (Tc) temperatures were determined from the thermograms.

2.6. Fourier Transform Infrared Spectroscopy (FTIR)

FTIR analysis was performed using a TA Instruments spectrometer with an ATR accessory to characterize functional groups in PLA and PLA/FsHAp composites. About 7 mg of each sample was placed on the ATR crystal, and spectra were collected over 4000–600 cm^{-1} to identify characteristic bonds.

2.7. Morphology

Surface morphology of neat PLA and PLA/FsHAp composites was observed using a JEOL JSM-6400 SEM after sputter-coating the samples with a thin gold layer to minimize charging.

3. RESULTS AND DISCUSSION

3.1. Mechanical Properties

The mechanical behavior of PLA/FsHAp composites was evaluated through tensile, flexural, and impact testing as described below.

3.1.1. Tensile Properties

Figure 2 presents the influence of FsHAp loading on the tensile strength of PLA/FsHAp composites. Neat PLA showed the highest strength (64.4 MPa), while the incorporation of FsHAp (10 to 30 wt%) generally reduced tensile strength. This reduction is mainly linked to the incompatibility between hydrophobic PLA and hydrophilic FsHAp, promoting filler agglomeration and weakening interfacial adhesion [14]. At 10 wt% FsHAp, the composite recorded the lowest strength (55.1 MPa), likely due to poor dispersion and limited reinforcement. Increasing the filler content to 20 wt% improved strength to 58.1 MPa, suggesting better dispersion and stronger reinforcement at this level. However, at 30 wt%, tensile strength decreased again (56.2 MPa), attributed to renewed agglomeration and stress concentration, leading to compromised structural integrity. Similar trends have been reported in earlier studies, where excessive FsHAp loading promoted premature failure due to poor interfacial bonding and stress localization [15].

Figure 3 shows the variation of Young's modulus in PLA/FsHAp composites with filler loadings up to 30 wt%. Neat PLA displayed the lowest modulus (1490 MPa), while incorporation of FsHAp led to a steady increase, reaching 2522 MPa at 30 wt%, a 69% improvement. This enhancement is attributed to effective filler dispersion within the PLA matrix, which increases stiffness and brittleness, thereby improving rigidity. The reinforcing effect of FsHAp contributes to higher structural integrity and modulus [15]. Although this trend contrasts with some studies reporting negligible or adverse effects of FsHAp addition [16], it is consistent with reports where higher FsHAp content enhanced the modulus of PLA composites [17].

Figure 4 presents the elongation at break of PLA/FsHAp composites as a function of FsHAp filler content. In general, incorporating rigid fillers like FsHAp into the PLA matrix leads to a reduction in elongation at break [7]. Pure PLA exhibited an elongation at break of 6.24%, indicative of ductile failure. Upon the addition of FsHAp

fillers, the deformation behaviour shifted markedly, with a noticeable transition to brittle behaviour occurring at around 10 wt% FsHAp, where the elongation at break dropped to 4.66%.

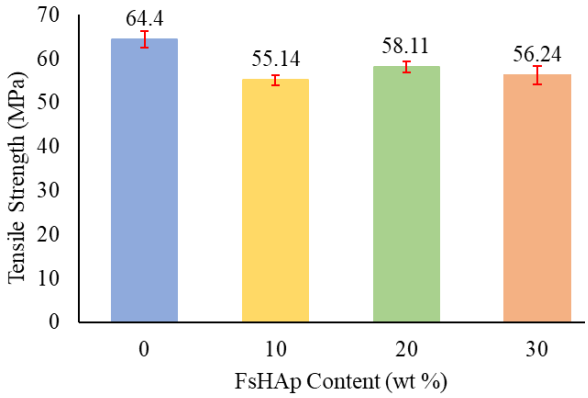

Fig. 2. Tensile strength of PLA/FsHAp composites at varying FsHAp filler content

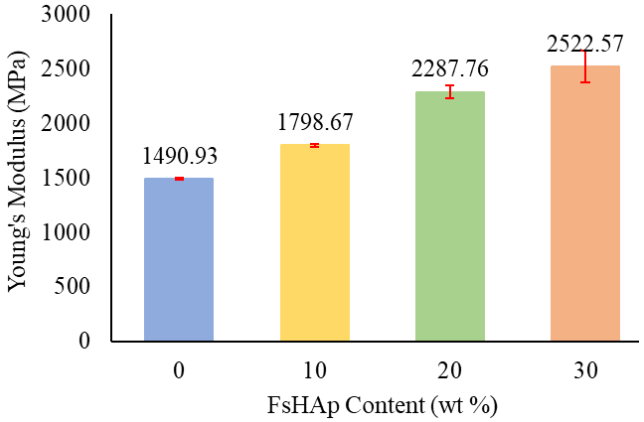

Fig. 3. Young's modulus of PLA/FsHAp composites at varying FsHAp filler contents

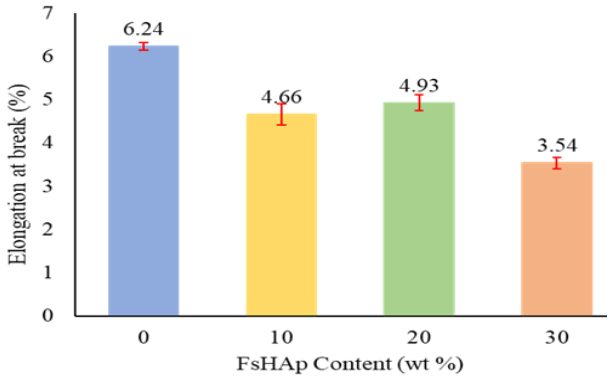

Fig. 4. Elongation at break of PLA/FsHAp composite at varying FsHAp filler content

According to Pawarangkool and Keawwattana [14], such composite failures typically originate at the interface between the FsHAp fillers and the PLA matrix. Interestingly, at 20 wt% FsHAp content, the elongation at break increased slightly to 4.93%, likely due to a more homogeneous dispersion of FsHAp within the matrix, which may have improved interfacial adhesion and stress distribution. This observation is consistent with the tensile strength data, which also showed enhancement at 20 wt% FsHAp. However, at 30 wt% FsHAp content, the elongation at break decreased again to 3.54%. This decline is attributed to the agglomeration of FsHAp particles,

leading to reduced contact areas and the formation of microstructural defects, which compromise the overall flexibility and stiffness of the composite.

3.1.2. Flexural properties

Figure 5 presents the influence of FsHAp filler loading on the flexural strength of PLA/FsHAp composites. Pure PLA displayed the highest flexural strength of 117.5 MPa, while the composite containing 30 wt% FsHAp showed the lowest value at 90.9 MPa. The reduction at higher filler content is associated with poor particle dispersion and increased viscosity, which hinders effective stress transfer. At 10 wt% FsHAp, the flexural strength dropped noticeably to 93.6 MPa. In contrast, an improvement was recorded at 20 wt% FsHAp, where the value increased to 99.6 MPa, likely due to more uniform filler dispersion that enhanced interfacial adhesion and load transfer. The observed trend is consistent with the tensile strength results, with the 20 wt% FsHAp composites achieving the best performance in both properties. The significant decline at 30 wt% FsHAp is mainly attributed to particle agglomeration, which weakens bonding at the filler–matrix interface and reduces overall mechanical integrity.

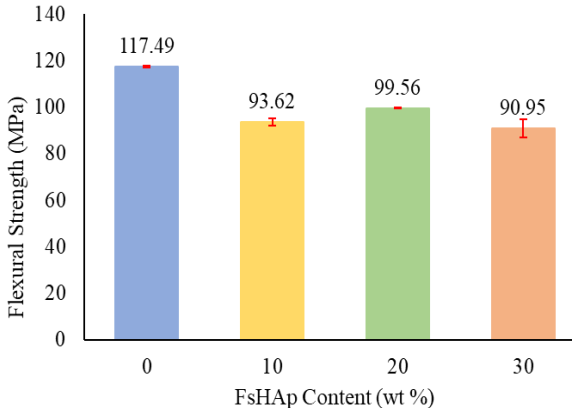

Fig. 5. Flexural strength of PLA/FsHAp composite at varying FsHAp filler content

Figure 6 shows the variation in flexural modulus of PLA/FsHAp composites with different filler loadings. The modulus increased markedly from 3821 MPa for neat PLA to 5107 MPa at 30 wt% FsHAp, representing an improvement of about 33%. This increasing trend agrees with the results reported by Ferri et al. [17], who observed a progressive rise in flexural modulus with higher FsHAp content. The findings suggest that incorporating FsHAp effectively enhances the stiffness of PLA-based composites.

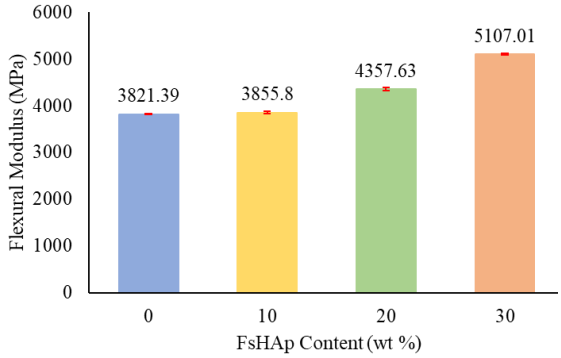

Fig. 6. Flexural modulus of PLA/FsHAp composite at varying FsHAp filler content

3.1.3. Impact properties

Figure 7 depicts the impact strength of PLA/FsHAp composites at different filler loadings. Neat PLA recorded an impact strength of 2.8 kJ/m², reflecting its limited capacity for energy absorption due to its inherent brittleness and low plastic deformation before fracture [17]. With the addition of FsHAp, the impact strength gradually increased, reaching the highest value of 3.1 kJ/m² at 20 wt%. This improvement is likely attributed to better dispersion of FsHAp particles within the PLA matrix, which enhanced energy dissipation during fracture [4].
However, a significant decline in impact strength was observed at 30 wt% FsHAp, dropping to 1.48 kJ/m², about 113% decrease compared to the 20 wt% formulation. This reduction is attributed to particle agglomeration at higher filler contents, leading to poor dispersion and the formation of stress concentration sites within the PLA matrix. Such agglomerates hinder effective stress transfer and reduce the interaction between PLA chains [15].

Therefore, 20 wt% FsHAp filler content appears to be the optimum composition, providing the highest impact strength among all tested formulations, likely due to enhanced dispersion and interfacial bonding within the composite.

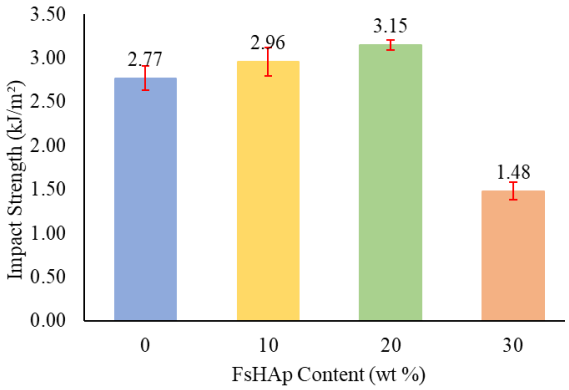

Fig.7. Impact strength of PLA/FsHAp composites at varying FsHAp filler content

3.2. Microstructure Properties

Figure 8 presents the fracture surface morphologies of neat PLA, PLA/FsHAp10, PLA/FsHAp20, and PLA/FsHAp30 composites. The fracture surface of pure PLA (Figure 8a) appears relatively smooth, a typical feature of brittle failure with limited plastic deformation. In contrast, incorporating FsHAp fillers produced rougher surfaces with noticeable porosity and voids. At 10 wt% and 20 wt% filler loadings (Figures 8b and 8c), the composites show a more refined and uniform distribution of spherical FsHAp particles within the PLA matrix. The spherical particle geometry promotes better dispersion despite some degree of agglomeration, which is expected due to the wide particle size distribution [17]. This improved dispersion enhances interfacial adhesion between the filler and matrix, enabling more effective stress transfer and improved mechanical properties [19]. Notably, the microstructural observations at 20 wt% FsHAp correspond closely with the tensile, flexural, and impact test results, confirming that this composition provides the most favorable dispersion and performance.

Furthermore, a noticeable agglomeration of FsHAp particles within the PLA matrix was detected, particularly at the 30 wt% filler content. These clusters act as stress concentration sites, which promote crack initiation and premature failure [15]. The presence of irregularly shaped aggregates hinders effective particle interlocking and entanglement, resulting in poor dispersion of the filler throughout the matrix. Consequently, the composite exhibits reduced energy absorption during impact, leading to diminished mechanical performance [17]. The SEM observations for the 30 wt% FsHAp formulation are consistent with the declines in tensile, flexural, and impact strength, confirming that excessive filler loading adversely affects composite properties.

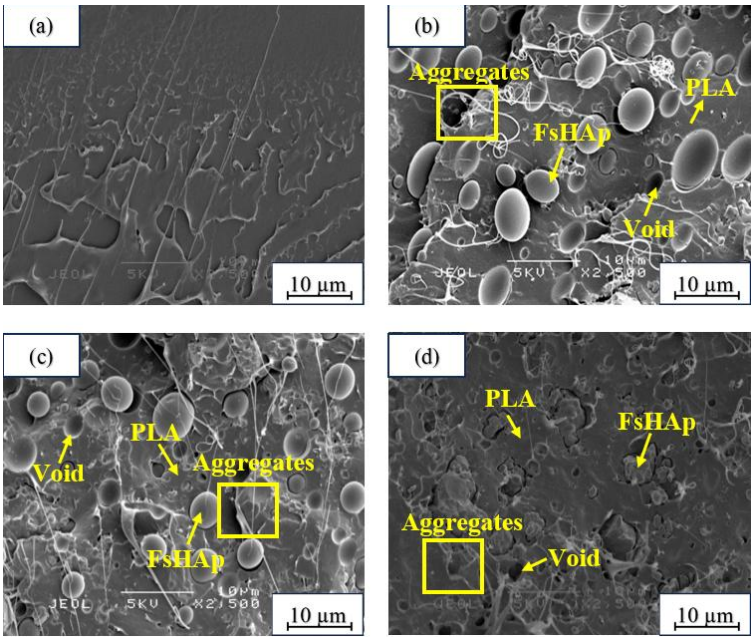

Fig. 8. SEM micrographs of impact fracture surface of (a) PLA, (b) PLA/FsHAp10, (c) PLA/FsHAp20 and (d) PLA/FsHAp30.

3.3 Chemical and Thermal Properties

3.3.1. Chemical Analysis Using FTIR

The FTIR spectra of neat PLA and PLA/FsHAp composites are presented in Figure 9. In the spectrum of pure PLA (Figure 9a), a distinct band appears at ~2944 cm^{-1}, corresponding to CH_3 stretching vibrations. Characteristic ester-related peaks are also observed at 1747 cm^{-1}, 1180 cm^{-1}, 1080 cm^{-1}, and 1042 cm^{-1} [4]. Among these, the sharp absorption at 1747 cm^{-1} is attributed to C=O stretching, while the band at 1264 cm^{-1} is associated with C–H bending in the PLA backbone. Additionally, a peak at 868 cm^{-1} indicates OH bending vibrations [4].

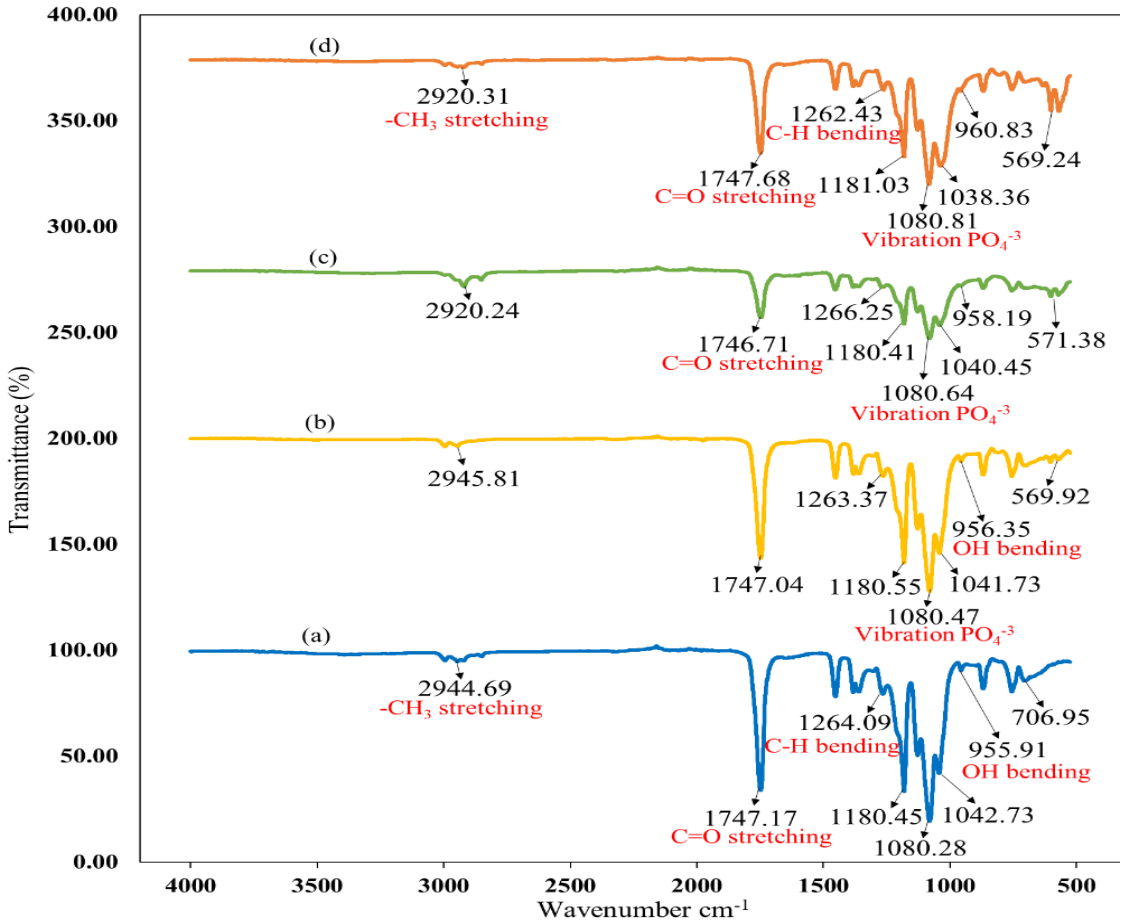

Fig. 9. FTIR spectrums of (a) PLA, (b) PLA/FsHAp10, (c) PLA/FsHAp20 and (d) PLA/FsHAp30

Figures 9(b), (c), and (d) present the FTIR spectra of PLA/FsHAp composites containing 10, 20, and 30 wt% FsHAp, respectively. Notably, the C=O stretching band at 1746 cm^{-1} exhibited a slight shift toward lower wavenumbers, particularly in the composite with 20 wt% FsHAp, suggesting the presence of chemical interactions between the FsHAp filler and the PLA matrix [19]. Furthermore, the PO_4^{3-} vibrational stretching band became increasingly prominent with higher FsHAp content. Specifically, for the 30 wt% FsHAp composites, the PO_4^{3-} peak was observed at 569 cm^{-1}, while in the 10 wt% composite, this peak appeared at a slightly higher wavenumber (571 cm^{-1}), indicating interactions between phosphate groups and the PLA matrix. These spectral changes are likely associated with improved dispersion of FsHAp particles and enhanced matrix–filler interactions [20]. Additionally, the emergence of new C–H bending bands further supports the occurrence of additional molecular interactions between the PLA and FsHAp components [20]. In contrast, although the 30 wt% FsHAp composites exhibited the most intense PO_4^{3-} peak and pronounced spectral features from both PLA and FsHAp, this was likely due to particle agglomeration, which may have reduced the extent of interfacial interaction between the matrix and filler.

3.3.2. Thermal Properties Using DSC

Figure 10 presents the DSC thermograms of neat PLA and PLA/FsHAp composites, illustrating their glass transition (Tg) and melting behavior (Tm). Among the formulations, the 30 wt% FsHAp composite displayed the

highest Tg at 58.3 °C. The addition of 10 and 20 wt% FsHAp increased the stiffness of the PLA matrix and restricted chain mobility [21], which may explain the absence of a distinct Tg peak in their DSC profiles. In contrast, at 30 wt% loading, a clear Tg signal was detected at 58.4 °C, indicating weaker polymer–filler interactions at higher filler concentrations. Similar to the findings of Albano et al. [22], this behavior suggests that interfacial interactions or non-covalent bonding between FsHAp and PLA chains contribute to reduced chain mobility, thereby modifying the thermal transitions.

The melting temperature (Tm) of neat PLA was slightly higher than that of the composites containing 10 and 20 wt% FsHAp, while the 30 wt% formulation exhibited only a minimal difference compared to neat PLA. The reduction in Tm at lower filler loadings is attributed to the disruption of chain packing and the formation of structural imperfections within PLA crystallites. As noted by Puteri Marzuki et al. [23], the melting characteristics of PLA/HAp systems depend on factors such as HAp particle size and the degree of lamellar crystalline perfection, which may develop both at the filler interface and within the polymer matrix. These irregularities contribute to a decrease in Tm. The small variation in Tm between the 10 and 20 wt% composites suggests only a limited effect of filler content on the crystalline order of PLA at these levels. Likewise, the negligible change at 30 wt% indicates reduced filler–matrix interactions at higher loadings.

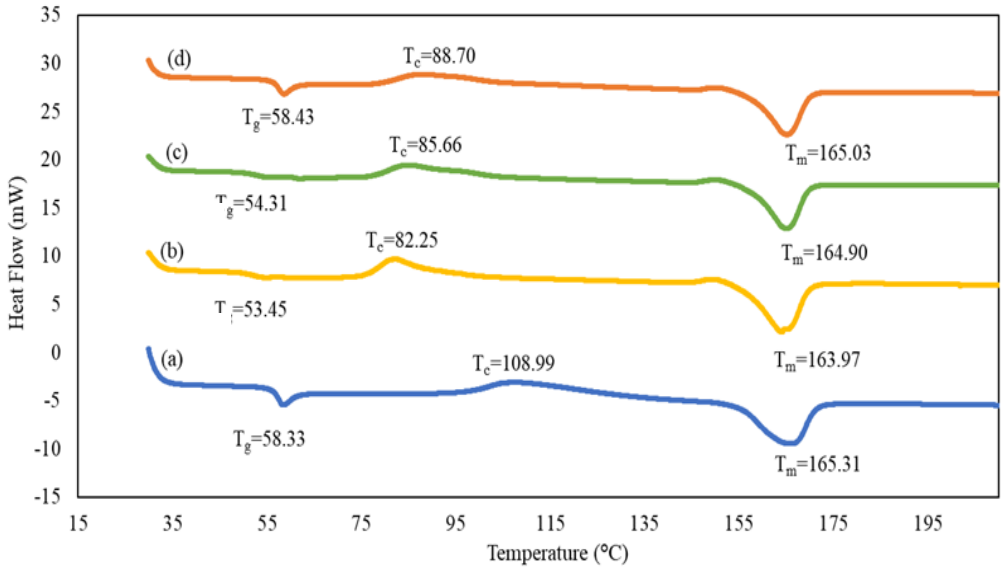

Fig. 10. DSC thermograms of (a) PLA, (b) PLA-10FsHAp, (c) PLA-20FsHAp and (d) PLA-30FsHAp

In terms of crystallization, pure PLA exhibited the highest crystallization temperature (Tc) at 108.9 °C, whereas all composites showed lower Tc values. This decrease is linked to the role of FsHAp in inducing heterogeneous nucleation, which dilutes the available polymer chains and decreases overall crystallinity [24]. Interestingly, within the composites, Tc increased gradually with rising filler content (10–30 wt%). This behavior can be explained by the restriction of chain mobility imposed by FsHAp particles; as filler loading increases, the reduced interparticle spacing further limits chain movement, slowing crystallization kinetics and resulting in a higher Tc.

4. CONCLUSIONS

PLA/FsHAp composites with different filler loadings were successfully prepared using a twin-screw extrusion method. The FsHAp powder (5–10 μm) acted as an effective reinforcement for the PLA matrix. Among the studied formulations, the composite containing 20 wt% FsHAp showed the best overall performance, recording the highest tensile strength (58.1 MPa) and impact strength (3.1 kJ/m²). These enhancements are attributed to the well-dispersed FsHAp particles and strong interfacial bonding with the PLA matrix, as evidenced by SEM and FTIR analyses. The improved filler–matrix interface facilitated more efficient stress transfer and energy absorption, making the 20 wt% formulation particularly promising for biomedical uses that demand high impact resistance, such as bone fixation devices.

At higher filler loading (30 wt%), agglomeration and irregular particle morphology were observed, which reduced dispersion quality and negatively affected the mechanical response. Thermal analysis revealed slight decreases in glass transition and melting temperatures with increasing FsHAp content; however, the composites maintained stable thermal behaviour at 30 wt%, suggesting their suitability for physiological environments (~37 °C).

Overall, the PLA/20 wt% FsHAp composite offers the most favourable balance between mechanical strength and thermal stability, identifying it as a strong candidate for biomedical applications.

Author contributions: Che Nor Aiza Jaafar was responsible for the conceptualization of the study, drafting the manuscript, and conducting data analysis. Charles Christopher Sorrell provided supervision and was involved in the review and editing process. Prevenaa Rajendran contributed to data acquisition and interpretation. Ismail Zainol and Yue Jiang were involved in data interpretation and analysis. All authors have read and approved the final version of the manuscript.
Funding: This research was supported by the Department of Mechanical and Manufacturing Engineering, UPM. We thank Universiti Putra Malaysia for their support during the research.
Conflicts of Interest: There is no conflict of interest.

5. REFERENCES

[1] Evangelia B., Vasileios D., Georgia K., Theocharis K., Myrika S., Nikolaos D. B., Antonios V., Ioanna K. Dimitrios N. B., (2021), *Poly(lactic Acid): A Versatile Biobased Polymer for the Future with Multifunctional Properties—From Monomer Synthesis, Polymerization Techniques and Molecular Weight Increase to PLA Applications,* Polym., 13(11), 1822.
[2] Lopes M. S., Jardini A. L., Filho R. M., (2012), *Poly (lactic acid) production for tissue engineering applications*, Procedia Eng., 42, 1402–1413.
[3] Farah S., Anderson D. G., R. Langer, (2016), *Physical and mechanical properties of PLA, and their functions in widespread applications — A comprehensive review,* Adv. Drug Deliv. Rev., 107, 367–392.
[4] Custodio C. L., Broñola P. J. M., Cayabyab S. R., Lagura V. U., Celorico J. R., Basilia B. A., (2021), *Powder Loading Effects on the Physicochemical and Mechanical Properties of 3D Printed Poly Lactic Acid/Hydroxyapatite Biocomposites,* Int. J. Bioprinting, 7(1), 112–122.
[5] Li H., Huneault M. A., (2008), *Crystallization of PLA/Thermoplastic Starch Blends*, Int. Polym. Process., 235, 412–418.
[6] Hussain C. M., Thomas S., (2021), Handbook of Polymer and Ceramic Nanotechnol., Springer.
[7] Peremel S., Jaafar C.N.A, Zainol I., Ariffin M. K.A. M., Chen R. S., (2023), T*he Properties of Poly(lactic Acid) (PLA)/Hydroxyapatite (FsHAp) Composites Prepared Through Solvent Casting Techniques*, Malays. J. Microsc., 19(1), 43–54.
[8] Pietrzykowska E. Mukhhovskyi R., Chodara A., Wojnarowicz J., Kolstov I., Chudoba T., Lojkowsi W, (2019), *Composites of polylactide and nano-hydroxyapatite created by cryomilling and warm isostatic pressing for bone implants applications*, Mater. Lett., 236, 625–628.
[9] Z. Wang, C. Huang, J. Wang, B. Zou, C. A. Abbas, X. Wang, (2020), *Design and Characterization of Hydroxyapatite Scaffolds Fabricated by Stereolithography for Bone Tissue Engineering Application*, Procedia CIRP, 89, 170–175.
[10] Annisa, T., Azkiya, A., Fauzi, R. N., Nandiyanto, A. B. D., Hofifah, S. N. (2021). *Cost analysis and economic evaluation for manufacturing hydroxyapatite nanoparticles from eggshell waste*, Int. J. Res. Appl. Technol, 1(1), 211–226.
[11] Zainol, I., Alwi, N. M., Abidin, M. Z., Haniza, H. M. Z., Ahmad, M. S., Ramli, A. (2012). *Physicochemical properties of hydroxyapatite extracted from fish scales*, Adv. Mater. Res., 545, 235–239
[12] Zainol, I., Zainurin M. A. Z., Bakar N. H. A., Jaafar C. N. A., Mudhafar M., (2022), *Characterisation of porous hydroxyapatite beads prepared from fish scale for potential bone filler applications*, Malays. J. Microsc, 18(2), 48–57.
[13] Jaafar, C. N. A., Zainol, I., Khairani, M. I. I., Dele-Afolabi, T. T. (2022). *Physical and mechanical properties of tilapia scale hydroxyapatite-filled high-density polyethylene composites*, Polymers, 14(2), 251, https://doi.org/10.3390/polym14020251
[14] Pawarangkool, K., Keawwattana, W. (2013). *Study the Effect of the Addition of HAp from Crocodile Bones on the Mechanical Properties of PLA/HAp Composites.* Adv. Mater. Res., 834–836, 237–240.
[15] Tazibt, N., Kaci, M., Dehouche, N., Ragoubi, M., Atanase, L. I. (2023). *Effect of filler content on the morphology and physical properties of poly(lactic acid)-hydroxyapatite composites*, Materials, 16(2), 809.
[16] Zhou, D. M., et al. (2022). *Strong and osteoconductive poly(lactic acid) biocomposites by high-shear liquid dispersion of hydroxyapatite nanowhiskers*. Nanocompos., 8(1), 24–33.
[17] Ferri, J. M., Jordá, J., Montanes, N., Fenollar, O., Balart, R. (2018). *Manufacturing and characterization of poly(lactic acid) composites with hydroxyapatite*, J. Thermoplast. Compos. Mater., 31(7), 865–881.
[18] Sadudeethanakul, S., Wattanutchariya, W., Nakkiew, W., Chaijaruwanich, A., Pitjamit, S. (2019). *Bending strength and biological properties of PLA-HA composites for femoral canine bone fixation plate*, IOP

Conference Series: Mater. Sci. Eng**,** 635(1).
[19] Cheang, P., Khor, K. A. (2003). *Effects of particulate morphology on the tensile behaviour of polymer-hydroxyapatite composites,* Mater. Sci. Eng. A, 345(1–2), 47–54.
[20] Nadarajan, V., Phang, S. W., Choo, H. L. (2020). *Fabrication of 3D-printed bone scaffold of natural hydroxyapatite from fish bones in polylactic acid composite*, AIP Conference Proceedings, 2233(1), 040004, https://doi.org/10.1063/5.0001497.
[21] Injorhor, P., Trongsatitkul, T., Wittayakun, J., Ruksakulpiwat, C., Ruksakulpiwat, Y. (2022). *Nano-hydroxyapatite from white seabass scales as a bio-filler in polylactic acid biocomposite: Preparation and characterization*. Polymers, 14(19), 4158.
[22] Albano, C., González, G., Palacios, J., Karam, A., Castillo, R. V., Covis, M. (2013). *Characterization of poly L-lactide/hydroxyapatite composite: Chemical, thermal and thermomechanical properties*, Revista de la Facultad de Ingeniería U.C.V., 28(3), 97-108.
[23] Marzuki, A. P., Ismail M. H., Salleh F. M, (2022). *Rheological properties of hydroxyapatite (HAp)/poly-lactic acid (PLA) composite at different weight percentages in producing 3D printing filament*. Conference Proceeding of Mechanical Engineering Research Day, Universiti Teknikal Malaysia Melaka, pp. 43–45.
[24] Akindoyo, J. O., Beg, M. D. H., Ghazali, S., Heim, H. P., Feldmann, M. (2018). *Impact modified PLA-hydroxyapatite composites – Thermo-mechanical properties*. Compos. Part A: Appl. Sci. Manuf., 107, 326–333.

Received: August 31th, 2025 / Accepted: November 24th, 2025 / Paper available online: December 20th, 2025